Journal of Materials Chemistry C

ROYAL SOCIETY OF CHEMISTRY

PAPER

View Article Online
View Journal | View Issue

Cite this: *J. Mater. Chem. C*, 2020, **8**, 6813

α-DTC$_{70}$ fullerene performs significantly better than β-DTC$_{70}$ as electron transporting material in perovskite solar cells†

Edison Castro, ‡*[a] Olivia Fernandez-Delgado, ‡[a] Albert Artigas,[b] Gerardo Zavala,[a] Fang Liu,[c] Antonio Moreno-Vicente,[d] Antonio Rodríguez-Fortea,[d] José D. Velasquez,[ae] Josep M. Poblet[d] and Luis Echegoyen*[a]

Received 17th March 2020,
Accepted 13th April 2020

DOI: 10.1039/d0tc01382j

rsc.li/materials-c

In this work, two new C$_{70}$ isomers, α and β bis(2-(thiophen-2-yl)ethyl)-C$_{70}$-fullerene mono-adducts (DTC$_{70}$), were synthesized, characterized and used as electron transporting materials (ETMs) in perovskite solar cells (PSCs). Our results show that the α isomer improves both the J_{sc} and FF values of the devices, when compared to the results for the β-isomer and to those for phenyl-C$_{70}$-butyric acid methyl ester (**PC$_{71}$BM**), used as control. Devices based on **α-DTC$_{70}$** achieved a power conversion efficiency (PCE) of 15.9%, which is higher than that observed with **PC$_{71}$BM** (15.1%).

Introduction

In the past few years, the development of PSCs has received special attention because of the fast improvement of their PCE, from 3.8% in 2009 to 25.2% in 2019,[1] easy fabrication procedures and low cost.[2,3] These materials are promising for the production of new devices with enhanced properties for commercial applications.[4–10]

Among the different device configurations, inverted p–i–n planar PSCs have emerged as a new alternative due to their simple device architecture and low temperature manufacturing processes, while still keeping considerably high performances.[11] Another advantage of planar inverted PSCs is their versatility regarding both the hole transporting materials (HTMs) and the ETMs.[12–16] In this regard, fullerenes are among the best ETMs in inverted PSCs because of their deep lying lowest unoccupied molecular orbital energies (LUMO) that match with the conduction band of the perovskite[17] and their ability to accept multiple electrons.[2,18] Additionally, due to their low reorganization energy, fullerenes can accelerate photoinduced charge separation and slow down charge recombination in the dark.[19]

One of the most used fullerene derivatives in PSCs fabrication is the phenyl-C$_{60}$-butyric acid methyl ester (PC$_{61}$BM), but many other fullerenes have been successfully incorporated in PSCs.[2,20] It is worth noting that the function of fullerenes in PSCs is not only limited to accepting and transporting electrons. A wide variety of fullerene derivatives bearing different functional groups have been used with several purposes: as ETM compact layers, as interfacial modification layers, as additives, as cathode buffer layers and as double layers.[2,3,20]

Charge recombination and hysteretic behaviour are some of the drawbacks that affect the performance of PSCs. Recently, it has been shown that the introduction of heteroatom-containing motifs on fullerene derivatives can effectively passivate the trap sites of the surface of the perovskite layer by interaction with undercoordinated Pb^{2+} cations.[21] As a result of this interaction, charge recombination and hysteresis can be supressed, thus improving the overall photovoltaic performance.[21] It has been reported that fullerene derivatives passivate the trap sites that present both on the surface and in the grain boundaries of the perovskite layer.[22,23]

The functionalization of fullerenes has been widely studied to improve their solubility as well as to modify and control their physical and optical properties.[23–26] When functionalizing C$_{70}$, different isomers can be obtained, making the purification process difficult. Some of us have reported that the use of an α-C$_{70}$ fulleropyrrolidine as the ETM improves the performance exhibited by a regioisomeric mixture. Such difference was attributed to the energy disorder provided by the different α, β and γ isomers present in the mixture. Similar results were

[a] *Department of Chemistry, University of Texas at El Paso, 500 West University Avenue, El Paso, TX 79968, USA. E-mail: eacastroportillo@utep.edu, echegoyen@utep.edu*
[b] *Institut de Química Computacional i Catàlisi (IQCC), Department de Química, Universitat de Girona, 17003 Girona, Catalonia, Spain*
[c] *Department of Chemistry, Columbia University, New York, New York 10027, USA*
[d] *Departament de Química Física i Inorgànica, Universitat Rovira i Virgili, Marcel·lí Domingo 1, 43007, Tarragona, Spain*
[e] *Departamento de Química, Facultad de Ciencias Naturales y Exactas, Universidad del Valle, A. A. 25360 Cali, Colombia*

† Electronic supplementary information (ESI) available. See DOI: 10.1039/d0tc01382j

‡ These authors contributed equally.

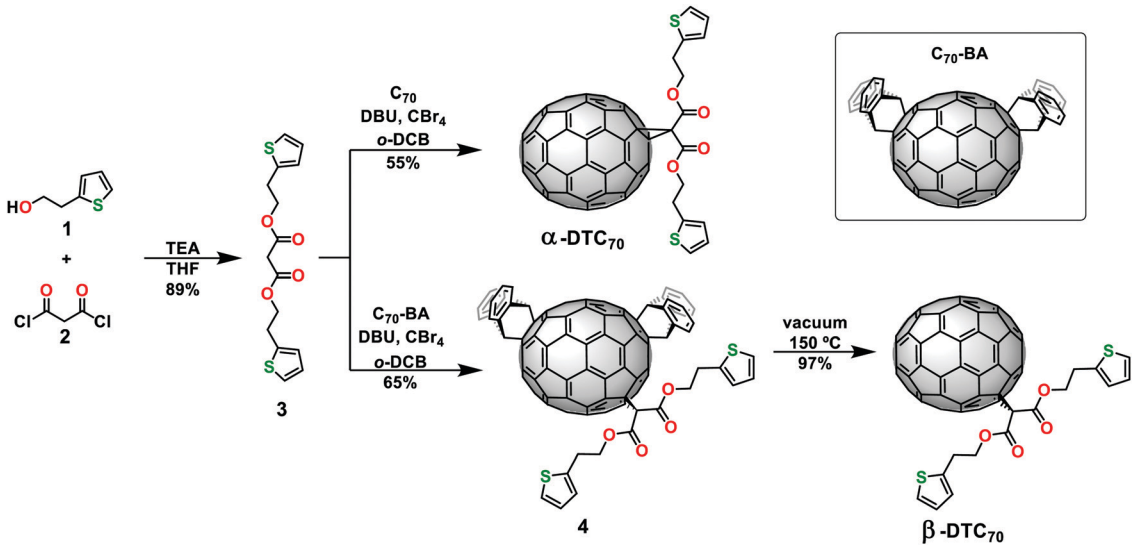

Scheme 1 Synthesis of **α-DTC$_{70}$** and **β-DTC$_{70}$**.

reported in other articles.[27–29] In general, the use of regioisomeric mixtures in photovoltaic devices often results in lower PCEs when compared to their corresponding pure isomers.[21,30–35] When comparing pure isomers to regioisomeric mixtures, most of the research so far has focused mainly on the α-isomer, which are more easily prepared than their β counterparts. Recently, we have reported a very straightforward methodology to selectively synthesize pure C_{70} β-isomers.[36] Additionally, we also reported that the introduction of thiophene moieties in the fullerene cage increases the interaction of the ETM and the perovskite layer, thus raising the photovoltaic performance. Here we report the synthesis and characterization of the α and β bis(2-(thiophen-2-yl)ethyl)-C_{70}-fullerene (DTC_{70}) mono-adducts and their performances in PSCs when used as the ETMs.

Results and discussion

The main motivation for this work was to probe the influence of the position of the functional groups in the two structurally different isomers and their impact on the photovoltaic performance as well as to gain a better understanding of their interaction with the perovskite layer. The **α-DTC$_{70}$** and **β-DTC$_{70}$** (Scheme 1) fullerene derivatives were synthesized according to our previously reported methodology.[36,37] The **α-DTC$_{70}$** isomer was prepared by a Bingel cyclopropanation reaction of malonate derivative **3** and fullerene C_{70}. The product was obtained in 55% yield after chromatographic purification. For the synthesis of the **β-DTC$_{70}$** isomer, C_{70} was first reacted with anthracene to yield the α-6-α′ C_{70}-BA isomer, which was used as a template to direct the subsequent cyclopropanation reaction to the C_s-symmetric tris-adduct isomer (**4**, Scheme 1). A thermal retro Diels–Alder reaction of **4** resulted in the selective synthesis of the **β-DTC$_{70}$** isomer with a 63% overall yield (see Materials and methods for details). The pure compounds were characterized by means of ^{1}H-NMR and ^{13}C-NMR spectroscopy, UV-Vis and matrix assisted laser desorption ionization-time of flight mass spectrometry (MALDI-TOF MS) (Fig. S1–S10, ESI†).

We recently reported that the functionalization of C_{60} with thiophene groups substantially improved their solubility in organic solvents such as chlorobenzene (CB), and PCE values higher than those of $PC_{61}BM$ based-devices were obtained for C_{60}-thiophene based devices. Additionally, devices fabricated with the compounds bearing the thiophene groups showed slower degradation, which was attributed to the specific interactions between the sulphur atoms present in the addend and the free lead cations from the surface of the perovskite layer.[37]

The feasibility of the **α-DTC$_{70}$** and **β-DTC$_{70}$** compounds to be used in inverted PSCs as ETMs was anticipated by estimation of their HOMO–LUMO energy values from UV-vis and cyclic voltammetry (CV) (Fig. S7 and S8, ESI†). Both isomers exhibited electrochemical and chemical reversibility evidenced by three well-defined and independent reduction and oxidation waves. The reduction onset potentials (E_{red}^{on}) for both isomers were estimated from the CV measurements using the equation LUMO = $-e(E_{red}^{on} + 4.8)$ (eV) and these are summarized in Table 1. The energy level diagram in Fig. 1a shows that the HOMO and LUMO energy levels of the new derivatives match well with that of the perovskite material. The two isomers exhibit deep enough HOMO values to block the holes and low enough LUMO values to allow the fast transport of electrons, indicating that they can be used efficiently as ETMs in PSCs.

X-ray diffraction (XRD) was performed to characterize the formation of the perovskite layer. As observed in Fig. S11 (ESI†) the perovskite is completely formed, as indicated by the characteristic

Table 1 Optical bandgap, onset reduction and HOMO/LUMO energy levels of **α-DTC$_{70}$** and **β-DTC$_{70}$**

Compound	λ_{abs} (nm)	E_g (eV)	E_{red}^{on} (V)	LUMO (eV)	HOMO (eV)
α-DTC$_{70}$	695	1.78	−0.92	−3.88	−5.66
β-DTC70	710	1.75	−0.93	−3.87	−5.62

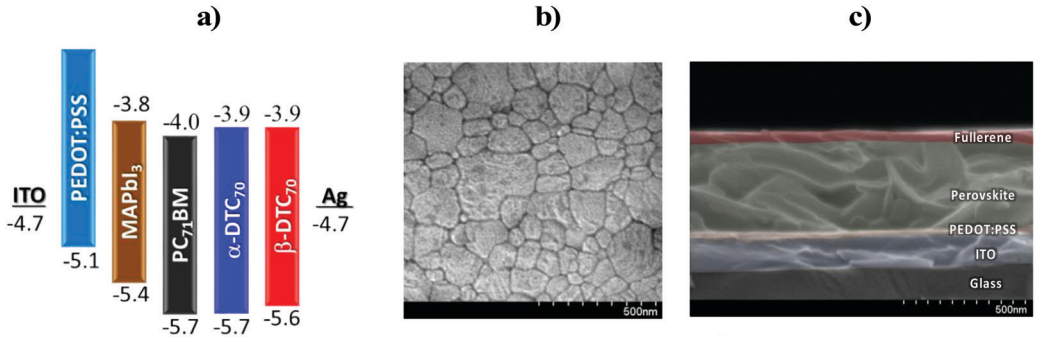

Fig. 1 (a) Energy level diagram, **$PC_{71}BM$** values were taken from the literature,[21] (b) surface SEM image of the perovskite layer and (c) cross section SEM of the perovskite device.

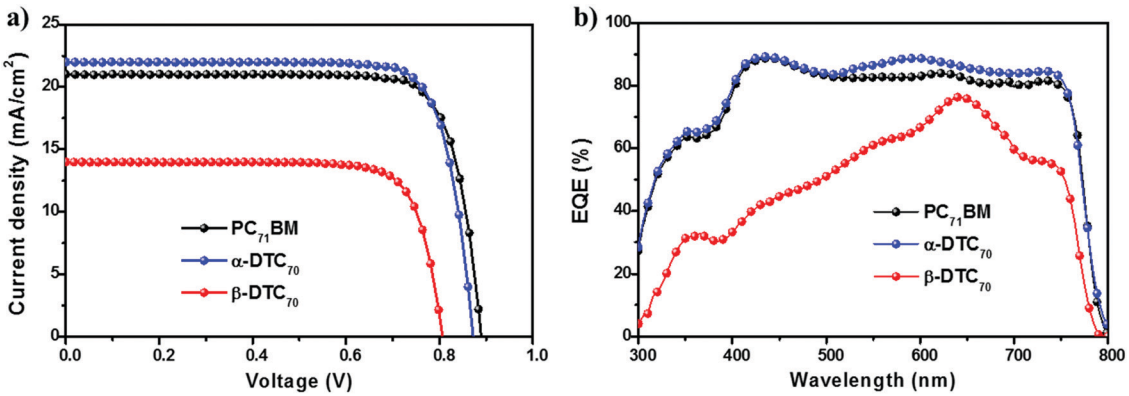

Fig. 2 (a) *J–V* curves and (b) EQE spectra of PSCs fabricated with **α-DTC_{70}**, **β-DTC_{70}** and **$PC_{71}BM$** as ETMs.

diffraction planes 100, 112, 211, 202, 220, 310, 312, 322 that suggest the formation of a tetragonal phase perovskite.[38] To study the quality of the films, scanning electron microscopy (SEM) was recorded to investigate the morphology of the perovskite layer, which revealed good homogeneity with no visible pin holes, and an average grain size of 200 nm (Fig. 1b). The cross-section SEM (Fig. 1c) measurements showed the indium tin oxide (ITO) transparent electrode (50 nm), poly(3,4-ethylenedioxythiophene): poly-styrene sulfonate (PEDOT:PSS) as HTM (25 nm), perovskite active layer (300 nm), and the fullerene ETL (80 nm).

To study the performance of **α-DTC_{70}** and **β-DTC_{70}** as ETMs, PSCs planar devices with an inverted configuration (ITO/PEDOT:PSS/perovskite/**α-DTC_{70}** or **β-DTC_{70}**/Ag) were fabricated. (see ESI,† for fabrication details).

Current–voltage (*J–V*) curves for both isomers and **$PC_{71}BM$** as control were obtained under AM 1.5G irradiation (100 mW cm^{-2}) in air. The photovoltaic parameters such as FF, J_{sc}, and V_{oc} are listed in Table 1. As shown in Fig. 2 and Table 2 a maximum PCE value of 15.9% was achieved for devices based on **α-DTC_{70}** whereas PCE values of 15.1% and 8.80% were obtained for **$PC_{71}BM$** and **β-DTC_{70}** based devices, respectively. The J_{sc} and FF values are higher for the α isomer, which is attributed to its good electron mobility (Fig. S13, ESI†) and high solubility in dichlorobenzene, whereas in the case of the β isomer the electron mobility is slightly lower. Although the differences are not very pronounced, the electron mobility follows the same trend as the PCE (Table S1, ESI†). It has been reported for similar C_{70} β isomers, that the packing in the solid state is not as compact and efficient as compared to the α isomer, yielding to a lower photovoltaic performance.[39]

Table 2 Summary of device performance. The calculated J_{sc} values were obtained from the EQE curves. Values in parentheses represent the best PCEs measured

Compound	Calculated J_{sc} (mA cm^{-2})	J_{sc} (mA cm^{-2})	V_{oc} (V)	FF	PCE (%)
$PC_{71}BM$	20.94	21.01	0.891	80.9	14.9 ± 0.3 (15.1)
α-DTC_{70}	21.95	22.00	0.874	82.6	15.3 ± 0.5 (15.9)
β-DTC_{70}	13.97	14.09	0.812	76.9	8.29 ± 0.5 (8.80)

Fig. S12 (ESI†) shows the PCEs based on statistical histograms obtained from 25 devices. The average efficiencies for **α-DTC_{70}**, **β-DTC_{70}** and **$PC_{71}BM$** based devices are 15.3% ± 0.5%, 8.29 ± 0.5% and 14.9% ± 0.3%, respectively, showing narrow distributions for the three compounds, which is an indicative of the good performance reproducibility.

The J_{sc} values were also investigated by external quantum efficiency (EQE) as shown in Fig. 2b. The values obtained from EQE were in agreement with the ones derived from the *J–V* curves, which suggest that the high J_{sc} and FF values for the **α-DTC_{70}** isomer can be related to a better ability to extract electrons in the visible spectral window. Also, we can conclude

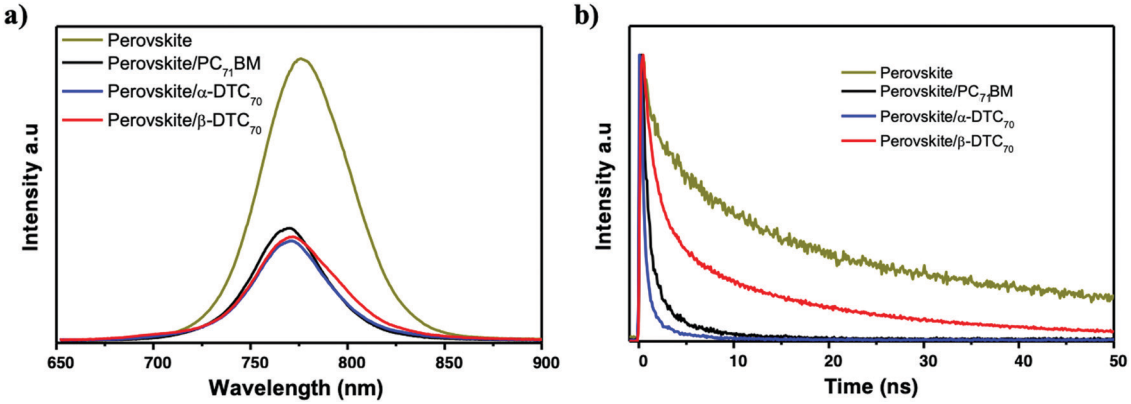

Fig. 3 (a) SSPL and (b) TRPL of the perovskite, perovskite/**α-DTC$_{70}$**, perovskite/**β-DTC$_{70}$** and perovskite/**PC$_{71}$BM** layers.

from the spectra that **α-DTC$_{70}$** can efficiently convert more than 80% of the incident photons into electrons in the visible range when compared to **β-DTC$_{70}$** and **PC$_{71}$BM**.

Steady state photoluminescence (SSPL) measurements and time resolved photoluminescence (TRPL) were performed to demonstrate that the α and β derivatives are good at extracting electrons, passivating the perovskite layer, and decreasing the electron–hole recombination. These measurements were collected from devices with the structure glass/perovskite and glass/perovskite/fullerene.

Fig. 3a shows that the perovskite layer exhibited a high PL signal, as the result of electron–hole recombination events, while the perovskite/fullerene devices showed a very efficient quenching of the photoluminescence, a clear indication of the ability of these compounds to reduce recombination processes. These results were very similar to those obtained for perovskite/**PC$_{71}$BM** devices. To study the kinetics of the electron–hole recombination, TRPL was also collected by monitoring the emission peak (780 nm) as a function of time. Fig. 3b shows that the decay time for **α-DTC$_{70}$** is faster than that of **PC$_{71}$BM** and **β-DTC$_{70}$**, which indicates that electrons are more efficiently transferred from the perovskite layer to **α-DTC$_{70}$** than to **β-DTC$_{70}$** or **PC$_{71}$BM**. These results could explain the devices performance since a faster decay time indicates a faster injection of electrons into the ETL, thus decreasing the recombination events.

To further investigate the electrical and charge transport properties at the perovskite/fullerene interface, electrochemical impedance spectroscopy (EIS) was performed for PSCs based on the new derivatives and **PC$_{71}$BM** (Fig. S14 and Table S2, ESI†). The equivalent circuit used to fit the Nyquist plots is illustrated in Fig. S14 (ESI†), where the series resistance (R_s) corresponds to the resistance of the two electrodes and the charge-transport resistance (R_{ct}) and the recombination resistance (R_{rec}) correspond to the resistances at the fullerene/perovskite interfaces.[40,41] Our results show that PSCs based on **α-DTC$_{70}$** display a lower R_{ct} and larger R_{rec} values than devices based on **β-DTC$_{70}$** and **PC$_{71}$BM**. Since very similar electron mobilities were measured for all the fullerene-based devices, the higher PCE values obtained for **α-DTC$_{70}$**-based devices must be the result of improved interfacial contact and charge transfer between the perovskite and the α-isomer. These results are also consistent with the higher PL quenching observed for perovskite/**α-DTC$_{70}$** films.

Stability studies were performed on unencapsulated devices under 50% humidity at ambient conditions. The devices were stable for up to 7 days and the ones containing **α-DTC$_{70}$** retained 80% of their initial PCE, compared to 42% and 40% for **β-DTC$_{70}$** and **PC$_{71}$BM**, respectively. As shown in Fig. 4, **α-DTC$_{70}$** devices showed comparatively better photostability than **β-DTC$_{70}$** and **PC$_{71}$BM** devices, which can be attributed to better packing in the solid state, thus allowing higher environmental resistance.

To better understand the interaction between **α-DTC$_{70}$** and **β-DTC$_{70}$** fullerene adducts and the perovskite surface, we performed periodic density functional theory (DFT) calculations. Previous studies on $PC_{61}BM$-like derivatives showed that these compounds interact with the surface *via* the fullerene and also *via* the addend.[38] The latter occurs through a direct interaction between the Pb^{2+} ions and the carbonyl or ester substituents. In the C_{70} adducts, the situation is similar but the lower symmetry of the C_{70} cage increases somewhat the complexity because of the possible different orientations of the addends with respect to the surface. Mono functionalization of C_{70} affords preferentially C_1–C_2 adducts (α type regioisomers), whereas the second most reactive bond is C_5–C_6, which yields β regioisomers.[42] As shown

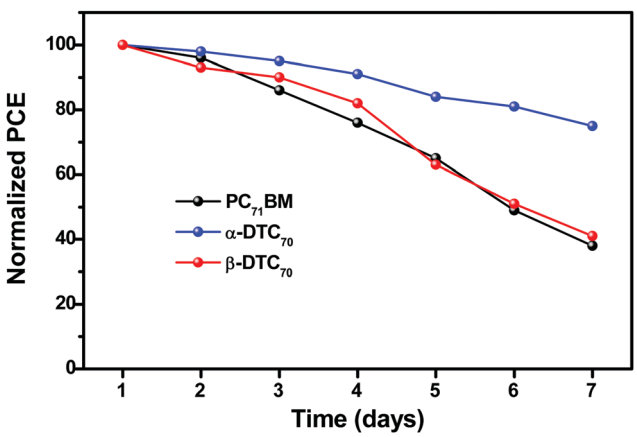

Fig. 4 Stability Studies of the PSCs fabricated with **α-DTC$_{70}$**, **β-DTC$_{70}$** and **PC$_{71}$BM** as the ETMs.

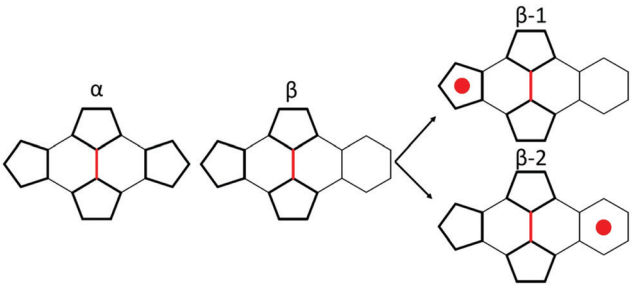

Fig. 5 α and β motifs for the [6,6] Bingel adducts of C_{70}. The red line represents the addend carbon–carbon bond position on the fullerene. For a more detailed representation of β_1 and β_2 isomers see Fig. S15 (ESI†).

in Fig. 5, α and β isomers exhibit different local symmetry, with the α isomer showing a symmetry plane through the C_1–C_2 (red) bond. It is worth mentioning that for **β-DTC$_{70}$** regioisomers, two different adsorption modes on the perovskite surface are possible depending on the way the C═O groups of the malonate are attached to the Pb^{2+} sites of the surface. We define the β-1 mode when the C═O group on the side of the pentagon is the one bonded to the Pb^{2+} atom, whereas the β-2 mode corresponds to the situation when the attached C═O is the one on the side of the hexagon (Fig. 5).

Table 3 collects adsorption energies and structural data for several orientations of fullerene adducts deposited on the perovskite surface. Initially, we have analyzed in detail the different orientations of a pristine C_{70} in contact with the surface. We have two fullerene alignments, cap and equatorial and three surface sites, hollow, top and bridge. Fig. S16 (ESI†) summarizes the adsorption energies computed for the different pristine C_{70} structures, which range between −1.07 eV and −1.81 eV. The optimal alignment corresponds to the fullerene interacting with a hollow site through the poles. The second most stable orientation is the bridge-equatorial one with an adsorption energy of −1.59 eV, only 0.22 eV higher than the lowest energy minimum. Indeed, for the **α-DTC$_{70}$** adduct, we have found that the most exothermic adsorption energy occurs when the fullerene is interacting at a bridge site, as shown in Fig. 6b.

Table 3 Adsorption energies and shortest distances for the different isomers of the fullerene adducts and adsorption sites

Isomer	E_{ads} [a]	RE [b]	d_{Pb-O} [c]	$d_{Surf-C_{70}}$ [d]
α-DTC$_{70}$-hollow	−1.90	0.67	2.869	3.138 < 3.226 < 3.411
α-DTC$_{70}$-top	−2.23	0.35	2.615	3.226 < 3.516 < 3.742
α-DTC$_{70}$-bridge	−2.36	0.22	2.638	3.100 < 3.304 < 3.679
β_1-DTC$_{70}$-hollow	−2.54	0.04	2.655	3.393 < 3.405 < 3.776
β_1-DTC$_{70}$-top	−2.43	0.15	2.709	3.175 < 3.394 < 3.640
β_1-DTC$_{70}$-bridge	−2.54	0.04	2.689	3.284 < 3.346 < 3.795
β_2-DTC$_{70}$-hollow	−2.01	0.57	2.857	3.315 < 3.338 < 3.528
β_2-DTC$_{70}$-top	−2.58	0.00	3.497	3.130 < 3.359 < 3.515
β_2-DTC$_{70}$-bridge	−2.48	0.10	3.009	3.201 < 3.516 < 3.526

[a] Adsorption energies in eV. [b] Relative energies with respect to β_2-DTC$_{70}$-top. [c] Shortest Pb–O distance in Å. [d] Shortest contacts between the carbon atoms of the fullerene and the perovskite surface in Å.

A similar analysis was done for the β regioisomers, for which we have found three orientations of the fullerene on the surface in an energy range of only 0.04 eV. The most exothermic adsorption energies are displayed by two β_1-DTC$_{70}$ adducts in hollow and bridge sites and one β_2 isomer on top. Indeed, β_2-DTC$_{70}$-top corresponds to the adduct with the shortest carbon-lead distance (3.130 Å). In β_1-DTC$_{70}$-bridge and β_1-DTC$_{70}$-hollow sites, the fullerene is found at longer separations from the surface, but the loss of interaction is compensated by the stronger Pb-addend interactions, revealed by shorter Pb–O distances (Table 3). Due to the small energy differences, it is reasonable to believe that in our device the β_1-DTC$_{70}$ isomers are occupying different adsorption sites on the perovskite surface.

The top and the hollow sites are less exothermic by 0.35 and 0.67 eV. The change in the fullerene orientation with respect to the pristine fullerene is due to the carbonyl-lead interaction that fixes the fullerene on the perovskite surface. The adsorption energies for the fullerene adducts are in general between 0.10 and 0.77 eV larger than in the pristine fullerene. This can be rationalized if we consider that the strong O–Pb^{2+} interactions easily overcome the loss of fullerene-surface interactions imposed by the addend constraints.

The electronic structure of lead-halide perovskites has been recurrently analyzed by means of DFT calculations showing that the valence band is mainly formed by antibonding states derived from hybridizations of 5p orbitals of iodine and 6s orbitals of lead, while the conduction band is mainly constituted by the empty 6p orbitals of lead.[43–46] Given that the electron transfer from the excited perovskite to the fullerene empty

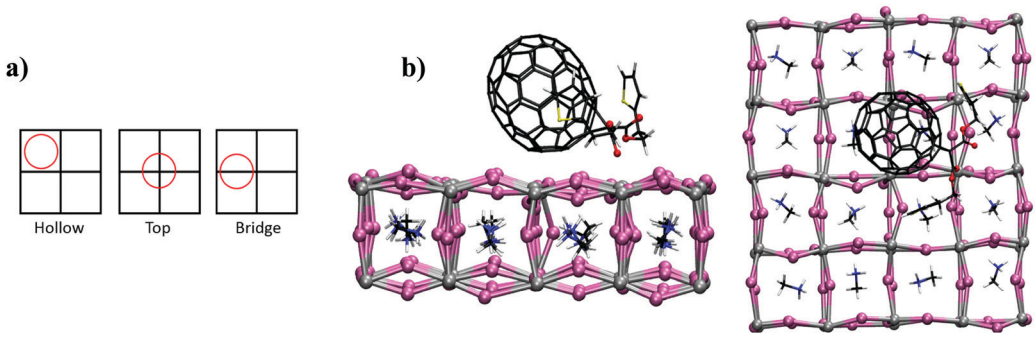

Fig. 6 (a) Schematic representation of three types of adsorption sites of the fullerene on the perovskite surface and (b) two views of the lowest energy structures (bridge isomer) for α-DTC$_{70}$.

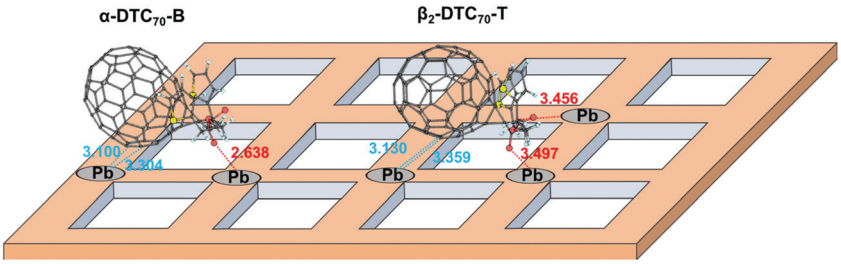

Fig. 7 Schematic representation for the lowest energy **α-DTC$_{70}$** and **β-DTC$_{70}$** adducts adsorbed on the MAPbI$_3$ surface. The values in cyan and red correspond to the shortest lead-fullerene and lead-addend distances (in Å), respectively. A 3D view of the metal adduct contacts can be found in Fig. S17 (ESI†).

orbitals has probably to involve the conduction band of the perovskite, we have analyzed the fullerene–lead contacts. In agreement with the experimental results, which exhibit a higher efficiency for the **α-DTC$_{70}$** isomer, Fig. 7 shows that the shortest contacts are observed for this isomer. Nevertheless, the contact distances between carbon atoms and lead are not very different and likely other factors, such as fullerene adduct compactness and packing could be relevant in the electron-transport and overall device performance properties.

Conclusions

In conclusion, we have regioselectively synthesized new α- and β-C$_{70}$ fullerene derivatives by following our previously reported methodology. The new compounds were fully characterized and tested in inverted PSCs as ETMs. Our results show significant differences between the isomers. The **α-DTC$_{70}$** exhibited an enhanced of the overall device performance with higher PCE, J_{sc} and FF values and a significantly improved ability to extract electrons as evidenced by PL. Additionally, the long term stability was also improved when devices were prepared with the α isomer, retaining 80% of the initial PCE for up to 7 days after fabrication. The different device performances of the two C$_{70}$ isomers was rationalized by DFT calculations. The electron mobilities together with EIS measurements, the packing differences reported in the literature between α and β isomers, and the DFT calculations in this article provide a reasonable rationalization for the drastically different PCEs observed experimentally.

Conflicts of interest

There are no conflicts to declare.

Acknowledgements

Authors thank the US National Science Foundation (NSF) for generous support of this work under CHE-1801317. The Robert A. Welch Foundation is also gratefully acknowledged for an endowed chair to L. E. (Grant AH-0033). Research reported in this paper was supported by the National Institute of General Medical Sciences of the National Institutes of Health under linked Award Numbers RL5GM118969, TL4GM118971, and UL1GM118970. Authors also thank Spanish Ministry of Science (grant CTQ2017-87269-P), the Generalitat de Catalunya (grant 2017SGR629) and the URV for support. J. M. P. also thanks ICREA foundation for an ICREA ACADEMIA award. The content is solely the responsibility of the authors and does not necessarily represent the official views of the National Institutes of Health.

References

1 NREL, Best Research-Cell Efficiencies, https://www.nrel.gov/pv/assets/pdfs/best-research-cell-efficiencies.20200218.pdf, accessed accessed March, 2020, 2020.
2 E. Castro, J. Murillo, O. Fernandez-Delgado and L. Echegoyen, *J. Mater. Chem. C*, 2018, **6**, 2635–2651.
3 Y. Fang, C. Bi, D. Wang and J. Huang, *ACS Energy Lett.*, 2017, **2**, 782–794.
4 M. A. Green, A. Ho-Baillie and H. J. Snaith, *Nat. Photonics*, 2014, **8**, 506.
5 M. Liu, M. B. Johnston and H. J. Snaith, *Nature*, 2013, **501**, 395.
6 M. D. McGehee, *Nat. Mater.*, 2014, **13**, 845.
7 A. Kojima, K. Teshima, Y. Shirai and T. Miyasaka, *J. Am. Chem. Soc.*, 2009, **131**, 6050–6051.
8 G. Xing, N. Mathews, S. Sun, S. S. Lim, Y. M. Lam, M. Grätzel, S. Mhaisalkar and T. C. Sum, *Science*, 2013, **342**, 344.
9 S. D. Stranks, G. E. Eperon, G. Grancini, C. Menelaou, M. J. P. Alcocer, T. Leijtens, L. M. Herz, A. Petrozza and H. J. Snaith, *Science*, 2013, **342**, 341.
10 C. Tian, E. Castro, T. Wang, G. Betancourt-Solis, G. Rodriguez and L. Echegoyen, *ACS Appl. Mater. Interfaces*, 2016, **8**, 31426–31432.
11 X. Liu, Y. Cheng, C. Liu, T. Zhang, N. Zhang, S. Zhang, J. Chen, Q. Xu, J. Ouyang and H. Gong, *Energy Environ. Sci.*, 2019, **12**, 1622–1633.
12 L. Tanghao, C. Ke, H. Qin, Z. Rui and G. Qihuang, *Adv. Energy Mater.*, 2016, **6**, 1600457.
13 E. H. Anaraki, A. Kermanpur, L. Steier, K. Domanski, T. Matsui, W. Tress, M. Saliba, A. Abate, M. Gratzel, A. Hagfeldt and J.-P. Correa-Baena, *Energy Environ. Sci.*, 2016, **9**, 3128–3134.
14 S. Yang, W. Fu, Z. Zhang, H. Chen and C.-Z. Li, *J. Mater. Chem. A*, 2017, **5**, 11462–11482.
15 H. Kim, K.-G. Lim and T.-W. Lee, *Energy Environ. Sci.*, 2016, **9**, 12–30.

16 L. Jiang, W. Gang, L. Kun, H. Xulin, Y. Qinyan, L. Cheng and M. Jun, *ChemPhysChem*, 2017, **18**, 617–625.
17 P. Schulz, E. Edri, S. Kirmayer, G. Hodes, D. Cahen and A. Kahn, *Energy Environ. Sci.*, 2014, **7**, 1377–1381.
18 L.-L. Deng, S.-Y. Xie and F. Gao, *Adv. Electron. Mater.*, 2017, 1700435, DOI: 10.1002/aelm.201700435.
19 H. Imahori and Y. Sakata, *Adv. Mater.*, 1997, **9**, 537–546.
20 T. Gatti, E. Menna, M. Meneghetti, M. Maggini, A. Petrozza and F. Lamberti, *Nano Energy*, 2017, **41**, 84–100.
21 E. Castro, G. Zavala, S. Seetharaman, F. D'Souza and L. Echegoyen, *J. Mater. Chem. A*, 2017, **5**, 19485–19490.
22 Y. Shao, Z. Xiao, C. Bi, Y. Yuan and J. Huang, *Nat. Commun.*, 2014, **5**, 5784.
23 C. Tian, E. Castro, G. Betancourt-Solis, Z.-A. Nan, O. Fernandez-Delgado, S. Jankuru and L. Echegoyen, *New J. Chem.*, 2018, **42**, 2896–2902.
24 A. Hirsch and M. Brettreich, *Fullerenes*, Wiley-VCH Verlag GmbH & Co. KGaA, Weinheim, Germany, 2004, pp. 383–415.
25 H. Andreas, *Angew. Chem., Int. Ed. Engl.*, 1993, **32**, 1138–1141.
26 Z. Slanina, *Fullerene Sci. Technol.*, 2000, **8**, 125–126.
27 T. Umeyama and H. Imahori, *Acc. Chem. Res.*, 2019, **52**, 2046–2055.
28 F. Zhang, W. Shi, J. Luo, N. Pellet, C. Yi, X. Li, X. Zhao, T. J. S. Dennis, X. Li, S. Wang, Y. Xiao, S. M. Zakeeruddin, D. Bi and M. Grätzel, *Adv. Mater.*, 2017, **29**, 1606806.
29 E. Castro, G. Zavala, S. Seetharaman, F. D'Souza and L. Echegoyen, *J. Mater. Chem. A*, 2017, **5**, 19485–19490.
30 W. W. H. Wong, J. Subbiah, J. M. White, H. Seyler, B. Zhang, D. J. Jones and A. B. Holmes, *Chem. Mater.*, 2014, **26**, 1686–1689.
31 K. X. Sun, Z. Lu, S. Zajaczkowski, W. Pisula, W. Hanssen, E. White, J. M. Williamson, R. M. Subbiah, J. Ouyang, J. Holmes, A. B. Wong and W. W. H. Jones, D. J, *Nat. Commun.*, 2015, **6**, 6013.
32 A. Mishra and P. Bäuerle, *Angew. Chem., Int. Ed.*, 2012, **51**, 2020–2067.
33 Y. Sun, C. Cui, H. Wang and Y. Li, *Adv. Energy Mater.*, 2012, **2**, 996.
34 M. Lenes, G.-J. A. H. Wetzelaer, F. B. Kooistra, S. C. Veenstra, J. C. Hummelen and P. W. M. Blom, *Adv. Mater.*, 2008, **20**, 2116.
35 T. Umeyama, T. Miyata, A. C. Jakowetz, S. Shibata, K. Kurotobi, T. Higashino, T. Koganezawa, M. Tsujimoto, S. Gélinas, W. Matsuda, S. Seki, R. H. Friend and H. Imahori, *Chem. Sci.*, 2017, **8**, 181–188.
36 M. R. Cerón, E. Castro, V. S. P. K. Neti, P. W. Dunk and L. A. Echegoyen, *J. Org. Chem.*, 2017, **82**, 893–897.
37 E. Castro, O. Fernandez-Delgado, F. Arslan, G. Zavala, T. Yang, S. Seetharaman, F. Dsouza and L. Echegoyen, *New J. Chem.*, 2018, **42**, 14551–14558.
38 O. Fernandez-Delgado, E. Castro, C. R. Ganivet, K. Fosnacht, F. Liu, T. Mates, Y. Liu, X. Wu and L. Echegoyen, *ACS Appl. Mater. Interfaces*, 2019, **11**, 34408–34415.
39 X.-X. Zhan, X. Zhang, S.-M. Dai, S.-H. Li, X.-Z. Lu, L.-L. Deng, S.-Y. Xie, R.-B. Huang and L.-S. Zheng, *Chem. – Eur. J.*, 2016, **22**, 18709–18713.
40 D. Liu, J. Yang and T. L. Kelly, *J. Am. Chem. Soc.*, 2014, **136**, 17116–17122.
41 A. Dualeh, T. Moehl, N. Tétreault, J. Teuscher, P. Gao, M. K. Nazeeruddin and M. Grätzel, *ACS Nano*, 2013, **8**, 362–373.
42 M. B. A. Hirsch, *Fullerenes: chemistry and reactions*, Wiley-VCH Verlag GmbH & Co, Germany, 2005.
43 M. Caputo, N. Cefarin, A. Radivo, N. Demitri, L. Gigli, J. R. Plaisier, M. Panighel, G. Di Santo, S. Moretti, A. Giglia, M. Polentarutti, F. De Angelis, E. Mosconi, P. Umari, M. Tormen and A. Goldoni, *Sci. Rep.*, 2019, **9**, 15159.
44 E. Mosconi, P. Umari and F. De Angelis, *Phys. Chem. Chem. Phys.*, 2016, **18**, 27158–27164.
45 L. M. Herz, *Annu. Rev. Phys. Chem.*, 2016, **67**, 65–89.
46 V. Blum, R. Gehrke, F. Hanke, P. Havu, V. Havu, X. Ren, K. Reuter and M. Scheffler, *Comput. Phys. Commun.*, 2009, **180**, 2175–2196.